MedChemComm

Accepted Manuscript

ROYAL SOCIETY OF CHEMISTRY

www.rsc.org/medchemcomm

1-[(2*E*)-3-phenylprop-2-enoyl]-1*H*-benzimidazoles as anticancer agents: Synthesis, crystal structure analysis and binding studies of the most potent anticancer molecule with serum albumin

Veerendra Kumar A. Kalalbandi, J. Seetharamappa*

Department of Chemistry, Karnatak University, Dharwad-580 003, India
*Corresponding author: E-mail:jseetharam@yahoo.com

Phone No.: +91-836- 2215286

Fax : +91-836-2747884

Abstract

A series of 1-[(2*E*)-3-phenylprop-2-enoyl]-1*H*-benzimidazoles have been synthesized and their ability to inhibit the growth of cancer cell lines has been investigated against NCI 60 cell panel. The compound 1-[(2*E*)-3-phenylprop-2-enoyl]-2-(4-chlorophenyl)-1*H*-benzimidazole (Compound **3f,** NSC: 773404/1) was found to display good antitumor activity against the nine tumor subpanels with the selectivity ratios ranging from 0.79 to 1.53 and from 0.47 to 1.69 at GI_{50} and TGI levels, respectively. Structural parameters of the potent anticancer active compound, **3f** have been studied from single crystal XRD data. Further, *in vitro* interaction of **3f** with transport protein, human serum albumin (HSA) was investigated by spectroscopic techniques. Static quenching mechanism was noticed in the binding of **3f** to HSA. Thermodynamic parameters revealed that the hydrogen bond and van der Waals forces played a major role in the interaction process.

Keywords: Anticancer activity; 1*H*-benzimidazoles; crystal structure; HSA; binding studies.

Introduction

In recent years, cancer is recognized as the leading disease that has posed a threat to human life. The world health organization has reported that the global cancer burden was doubled during the last 30 years of the 20th century.[1] The development of resistance against the prevailing anticancer drugs has generated more complication in the treatment of cancer[2,3] that keeps research window open in search of newer anticancer agents. However, the window passage has become narrower because it is rather more difficult to search a molecule that can selectively inhibit the proliferation of abnormal cells only with least or no effect on normal cells. Hence, investigation of a new chemical entity for the treatment of cancer assumes importance. Among several bioactive compounds, benzimidazoles still remain as potential bioactive molecules and construction of the benzimidazole pharmacophore may give a fruitful result in the investigation of cancer related drugs.[4,5]

Benzimidazole compounds have occupied a remarkable place among various heterocycles by virtue of their greater involvement in medicinal chemistry and drug discovery. Benzimidazoles are the key building block of numerous compounds that play a vital role in the functioning of bioactive molecules.[6] Different biological activities have been reported as these are structural isosteres of naturally occurring nucleotides that interact easily with biopolymers of the living system.[7] Substituted derivatives of benzimidazole exhibited noteworthy anticancer activities[8-10] besides a wide range of biological activities including antiviral,[11,12] antimicrobial,[13] anthelmintic,[14] anti-inflammatory[15] and antihistaminic[16] properties.

In addition to benzimidazoles, compounds containing cinnamoyl group are known to exhibit potent anticancer activity. Cinnamoyl group belongs to the class of auxin, which is recognized as the plant hormone regulating cell growth and differentiation.[17] The cinnamoyl functionality is also present in a variety of secondary metabolites of phenylpropenoid biosynthetic origin. The presence of α, β-unsaturated carbonyl moiety in cinnamoyl group would be considered as a Michael acceptor, which is an active group often employed in the design of efficient anticancer agents.[18] Further, the literature survey revealed that the compounds containing cinnamoyl group and cinnamoyl anthranilates exhibited significant anticancer activity.[19] In view of biological importance of cinnamoyl group, it was thought worthwhile to study the anticancer activity of the synthesized 1*H*-benzimidazole derivatives containing cinnamoyl group against NCI 60 cell panel.

Further, the interactions of benzimidazole derivatives and compounds containing cinnamoyl group with a biomolecule like HSA elucidated proper understanding of biological processes such as absorption, transportation, distribution, metabolism and excretion. It helps in designing new drug molecules. It is well-known that transportation and disposition of endogenous and exogenous ligands present in the blood are generally carried out by HSA.[20] Further, it has the capacity of binding reversibly to a large variety of small molecules that it serves as a carrier.[21] The affinity between a drug and HSA can alter the pharmacokinetics and pharmacodynamics of a drug. The drug that has either too high or too low affinity towards HSA would be rendered ineffective.[22,23]

In our recent work, we have reported the synthesis, characterization, anti-tubercular and cytotoxicity of 1-[(2*E*)-3-phenylprop-2-enoyl]-1*H*-benzimidazole derivatives.[24] Good results of preliminary studies encouraged us to investigate the anticancer activity of 1*H*-benzimidazole derivatives against NCI 60 cell panel and to carry out the interaction of the potent anticancer molecule with HSA.

Results and discussion

Synthesis and characterization of 1*H*-benzimidazoles

A series of 1-[(2*E*)-3-phenylprop-2-enoyl]-1*H*-benzimidazole derivatives were prepared as reported earlier (Fig. 1).[24] In brief, slow addition of freshly prepared cinnamoyl chloride to substituted benzimidazoles in dry THF in the presence of sodium hydride at 0-5 $^{\circ}$C yielded 1-[(2*E*)-3-phenylprop-2-enoyl]-1*H*-benzimidazole derivatives. The synthesized molecules were characterized by spectral methods. ^{1}H NMR spectra of all the compounds exhibited two doublets each around 6.12 - 7.20 ppm and 7.57 - 8.05 ppm. These were attributed to vinylic protons and the coupling constants of these protons ($^{3}J_{HH}$) at *ca* 16 Hz proved that these two protons were *trans* to each other. Further, all the aromatic protons were observed in the expected region. The ^{13}C NMR spectra of all the compounds exhibited signals around 128.9 - 133.4 ppm and 145.5 - 149.2 ppm due to vinylic carbon atoms. The carbonyl carbon appeared around 162.52 - 168.1 ppm and the aromatic carbon atoms were resonated in the expected region. Further, single crystals of 1-[(2E)-3-phenylprop-2-enoyl]-2-(4-chlorophenyl)-1*H*-benzimidazole were grown and X-ray studies were carried out to authenticate the structure.

Single crystal X-ray studies

Single crystal of the compound **3f** was developed from its alcoholic solution by slow evaporation. The ORTEP diagram of **3f** is presented in Fig. 2a. The developed crystals belonged to monoclinic system with a space group of $P2_1/c$. The unit cell parameters and crystal refinement[25] data of the compound, **3f** are given in Table 1.

Though there are no noteworthy hydrogen bonds in **3f** molecules, its molecules were stabilized by weak intermolecular C-H … N interactions in the solid state with a distance of 2.653 Å (Fig. 2b). The benzimidazole plane of **3f** makes a dihedral angle of 22.00 (3)º with cinnamoyl group due to steric hindrance of bulkier 4-Cl-phenyl ring. Further, 4-Cl-phenyl ring has a dihedral angle of 49.90 (3)º with the mean plane of benzimidazole ring system. Bond lengths and bond angles were observed to be in normal ranges. The data on bond lengths and bond angles, co-ordinates and displacement parameters have been deposited at Cambridge Crystallographic Data Centre (CCDC 1018656).

Anticancer activity

The synthesized compounds were submitted to National Cancer Institute (NCI), Bethesda, Maryland, USA, under the Developmental Therapeutic Program (DTP) for screening anticancer activity.[26] The screening comprises 60 human tumor cell lines (NCI60), representing leukemia, melanoma and cancers of the lung, colon, brain, ovary, breast, prostate and kidney.[27] The study involved two-stage process; firstly, the compounds were tested against 60 cell lines at a single dose concentration of 10^{-5} M. The compounds that exhibited a significant growth inhibition were tested at five concentration levels against the 60 cell panel. The compounds *viz*., **3a**(NSC: 773399/1), **3b** (NSC: 773400/1), **3c** (NSC: 773401/1), **3d** (NSC: 773402/1), **3e** (NSC:

773403/1), **3f** (NSC: 773404/1), **3g** (NSC: 773405/1) and **3h** (NSC: 773406/1) were subjected to full NCI 60 cell panel screening at a single dose (10^{-5} M).

Results of the single dose assessment are presented as a graph of mean growth percent of the treated cells. These results revealed both growth inhibition (between 0 and 100 growth percent) and cytotoxicity values (with less than 0 growth percent). The outputs from the single dose screening were analyzed by COMPARE program.[28] The compounds **3a**, **3d**, **3e**, **3g** and **3h** have displayed zero sensitivity while **3b** and **3c** exhibited low to moderate sensitivity. **3f** showed a considerable antiproliferative activity towards human tumor cell lines. The significant percentage growth inhibition (GI%) of the treated cells at 10^{-5} M concentrations of compounds are presented below: Compound **1b** (with 5,6-dimethyl substituent on benzimidazole): *Leukemia* CCRF-CEM (GI% 64.66), RPMI-8226 (GI% 63.61), SR (GI% 64.66),*Breast Cancer*MCF-7 (GI% 69.59); compound **1c**(with 6-methyl substituent on benzimidazole): *Leukemia* CCRF-CEM (GI% 60.81), RPMI-8226 (GI% 88.17), SR (GI% 84.70), *Colon Cancer* HCT-116 (GI% 64.84), *Breast Cancer* MCF-7 (GI% 73.43); compound **3f** (with 4-Cl-phenyl ring on C2-benzimidazole): *Leukemia* K-562 (GI% 60.22), MOLT-4 (GI% 78.07), *Non-Small Cell Lung Cancer* NCI-H460 (GI% 99.46), *Colon Cancer* HCC-2998 (GI% 94.92), *CNS Cancer* SNB-75 (GI% 81.93), *Melanoma* MALME-3M (GI% 84.12), *Ovarian Cancer* IGROV1 (GI% 89.62), OVCAR-4 (GI% 69.96), NCI/ADR-RES (GI% 89.22), SK-OV-3 (GI% 76.05), *Renal Cancer* TK-10 (GI% 81.42), *Prostate Cancer* PC-3 (GI% 93.91) DU-145 (GI% 88.87) and *Breast Cancer* MCF7 (GI% 89.71), HS 578T (GI% 80.03). However, the compound **3f** has showed a remarkable cytotoxic activity along with growth inhibition against most of the cancer

cell lines and corresponding results are depicted in Table 2. The compounds which reduced the growth of the cell lines to 32% or less were considered as *in vitro* active.[29,30] Thus, **3f** (NSC: 773404/1) satisfied pre-determined threshold growth inhibition criteria and so, was further selected for NCI full panel five dose assay at 10-fold dilutions of five different concentrations.

Anticancer activity at five dose concentrations

Five dose screening was carried out by evaluating the compounds against 60 cell lines representing 9 tumor subpanels at five different concentration levels (0.01, 0.1, 1, 10 and 100 μM). The results were expressed in terms of three response parameters GI_{50}, TGI and LC_{50}. These were obtained by plotting the values of log concentration versus % growth inhibition for all cell lines (Fig. 3). From Fig. 3, it is apparent that the compound **3f** completely inhibited the growth of ovarian cancer cell line NCI/ADR-RES. Further, this compound exhibited good to moderate anticancer activity against several examined cancer cell lines with GI_{50} values in the range of 0.38 - 3.13 μM. The acquired data (Table 3) revealed noticeable and remarkable sensitivity profile towards leukemia SR, melanoma LOX IMVI, leukemia RPMI-8226, leukemia CCRF-CEM, ovarian cancer OVCAR-8, breast cancer MCF-7, renal cancer UO-31, melanoma MDA-MB-435, ovarian cancer OVCAR-3, leukemia MOLT-4, renal cancer A498, renal cancer ACHN, colon cancer HCT-116, non-small cell lung cancer NCI-H522 and melanoma UACC-62 with GI_{50} values of 0.38, 0.59, 0.61, 0.73, 0.75, 1.01, 1.10, 1.11, 1.11, 1.13, 1.17, 1.18, 1.21, 1.23 and 1.27 μM respectively. From these results, it is evident that, the compound **3f** unveiled noteworthy sensitivity against leukemia, melanoma and renal cancer with average

sensitivity of a particular subpanel 1.06, 1.47 and 1.51 μM respectively. However, the criterion for selectivity of a compound depends upon the ratio obtained by dividing the average sensitivity of all cell lines (full panel) MID (μM) by their individual subpanel MID (μM). Ratios between 3 and 6 refer to moderate selectivity; ratios greater than 6 indicate higher selectivity towards the corresponding cell line, while compounds not meeting either of these criteria rated as non-selective.[31] In this context, compound **3f** was found to be non-selective; however managed to display a good antitumor activity against the nine tumor subpanels tested with selectivity ratios ranging from 0.79 to 1.53 and 0.47 to 1.69 at GI_{50} and TGI levels, respectively.

Structure activity relationship

Chew et al.[32] have recently demonstrated that α, β-unsaturated carbonyl moiety, also known as the Michael acceptor, can inhibit thioredoxin reductase through nucleophilic addition of glutathione cysteine-SH residues and can potentially be exploited for use at different concentrations in chemotherapeutic and chemopreventive strategies. With α, β-unsaturated carboxyl group, the synthesized benzimidazoles offer Michael-acceptor properties. Further, from the single dose results, it is clear that the compounds carrying activating groups *viz*., methyl, methoxy, phenyl and phenol groups on benzimidazole moiety did not enhance the anticancer activity while the compound containing 4-chlorophenyl group (**3f**) showed moderate to good antiproliferative activity. This suggested that the compounds having an electron-withdrawing group in the *para*-position of the phenyl ring were found to be more active to Michael addition.[33] The presence of 4-chloro phenyl ring on benzimidazole exhibited a better activity compared to rest of the synthesized molecules. However, it

is still preliminary to draw any conclusion that the Michael addition might be the only mode of action of these compounds. Finally, it is proposed that further derivatization of these compounds could result in obtaining more selective anticancer agents.

Interactions of compound 3f with human serum albumin

To understand the binding characteristics of the potent anticancer molecule **3f** with transport protein, HSA, we have employed fluorescence method.

Steady state fluorescence quenching studies

Fluorescence spectroscopy is the most suitable technique to investigate the interaction of a bioactive compound with a biomolecule[34] since it provides the information concerning the structural changes in the biomolecule upon interaction. We have investigated the interaction between the potent anticancer compound **3f** and serum albumin, HSA. HSA is the most abundant protein constituent of blood plasma and has been used as a model protein for diverse biophysical and physicochemical studies. It has a single tryptophan (Trp) residue (Trp-214) located in the hydrophobic cavity of the subdomain IIA of the so-called Sudlow's binding site I.[35] The intrinsic fluorescence of Trp residues is extremely sensitive to its environment and can be used to comprehend the binding of small molecules to protein.

Fluorescence quenching may be induced by a variety of molecular interactions with a quencher molecule. In the present study, the emission spectra of HSA in the presence and absence of increasing amounts of **3f** were recorded to examine the interaction between **3f** and HSA. Fig. 4 represents the concentration dependent quenching of protein fluorescence by **3f**. It could be clearly seen that HSA showed a strong emission band at 335 nm upon excitation at 280 nm. The compound **3f** did not

exhibit emission under the experimental conditions. Addition of **3f** to HSA led to a significant decrease in the fluorescence intensity besides the red shift in emission wavelength thereby suggesting the changes in the environment around HSA.

Fluorescence quenching may be either dynamic or static or both. The dynamic can be differentiated from the static quenching based on their dependence on temperature. Thus, to propose the fluorescence quenching mechanism, the fluorescence quenching titration was carried out at different temperatures (288, 298 and 308 K) and the results were analyzed using the Stern-Volmer equation[36] shown below:

$$F_0/F = 1 + K_{SV}[Q] = 1 + K_q\tau_0[Q] \quad (1)$$

where F and F_0 are the fluorescence intensities with and without the quencher, respectively, K_{SV} is the Stern-Volmer quenching constant, K_q is the biomolecular quenching constant, τ_0 is the average life time of biomolecule without the quencher and [Q] is the concentration of the quencher. The Stern-Volmer quenching constants were obtained from the plot of F_0/F versus [Q] and the corresponding results are tabulated in Table 4. The Stern-Volmer plots (Fig. 5) manifest the decreasing trend of K_{SV} with increase in temperature indicating the presence of static quenching mechanism.

Analysis of binding equilibria

When small molecules bind independently to a set of equivalent sites on macromolecules, it is possible to evaluate the binding constant and number of molecules binding to protein using the following equation:[37]

$$\log[(F_0-F)/F] = \log K + n \log[Q] \quad (2)$$

where K is the binding constant and n is the number of molecules of **3f** binding to albumin molecule. The values of K and n were calculated from the plot of log [(F_0-F)/F] versus log [Q] and the results are shown in Table 4. The magnitude of K indicated the strong binding between **3f** and HSA. Further, the values of K decreased with increase in temperature indicating the decreased stability of **3f**-HSA complex at higher temperatures. It was evident from the values of n that one molecule of **3f** bound to one molecule of HSA.

Thermodynamics of interaction and nature of the binding mode

The non-covalent interactions between the ligand and protein may include hydrophobic forces, electrostatic interactions, van der Waals interactions, hydrogen bonds etc.[38] The forces acting between small molecules and macromolecules can be proposed based on thermodynamic parameters, enthalpy change (ΔH°) and entropy change (ΔS°). Hence, to elucidate the mode of binding between **3f** and HSA, the temperature-dependence of the binding constant of **3f**-HSA was determined at different temperatures (288, 298 and 308 K). The thermodynamic parameters are evaluated using the following equation:

$$\log K = -\Delta H°/2.303RT + \Delta S°/2.303R \quad (3)$$

The plot of log K versus 1/T (Fig. 6) yielded the values of ΔH° and ΔS° and were found to be -132.0 $kJmol^{-1}$ and -356.1 $JK^{-1}mol^{-1}$ respectively. The values of ΔG° were calculated using the equation given below:

$$\Delta G° = -2.303RT \log K \quad (4)$$

From the thermodynamic stance, ΔH° > 0 and ΔS° > 0 proposes the hydrophobic interaction while ΔH° < 0 and ΔS° < 0 specifies the van der Waals forces and/or

hydrogen bond formation; and $\Delta H° \approx 0$ and $\Delta S° > 0$ reflects an electrostatic force.[39] Negative values of $\Delta H°$ and $\Delta S°$ (Table 4**)** observed in the present study revealed the presence of hydrogen bond and van der Waals forces in the binding process. Negative values of $\Delta G°$ indicated the spontaneity of the interaction between **3f** and HSA.

Site specific interaction

It is supposed that the compound that interacts to serum albumin binds at a series of relatively well-defined regions on the protein. Sudlow et al.[40] have proposed two discrete sites for binding on the protein *viz*., site I and site II. It is supposed that site I of albumin has the affinity for warfarin, phenylbutazone etc., while that of site II shows preferential affinity for ibuprofen, flufenamic acid etc. Digitoxin binding is recognized to be independent of sites I and II. Hence, competitive experiments were carried out to determine the site specificity of **3f** on HSA and their binding constants were calculated to be $3.50x10^3$, $5.63x10^3$ and $5.73x10^3$ M^{-1} for **3f-**HSA with phenylbutazone, ibuprofen and digitoxin respectively at 303 K. Significant decrease in the binding constant of **3f-**HSA in the absence of the site probe was found to be $5.68x10^3$ at 303 K. Decreased binding constant of **3f-**HSA in the presence of phenylbutazone suggested that the phenylbutazone was significantly displaced by compound **3f**. In other words, both of them compete for the same binding site in the protein. So, the site I located in subdomain II A was proposed to be the core binding site for **3f** in HSA.

Effects of common ions on binding of 3f-HSA

Some common ions are extensively dispersed in humans and animals, which can affect the interactions of compounds with serum albumin. So, metal ions may affect

the interactions of a drug with HSA and thus it may influence the distribution, pharmacological property and metabolism of medicine in the blood. In view of this, the binding of **3f** with HSA was investigated in the presence of common ions *viz*., Co^{2+}, Cu^{2+}, K^{+}, Mn^{2+}, Ni^{2+} and Zn^{2+} at 303 K. The corresponding binding constants shown in Table 5 revealed that the binding constant of **3f-**HSA decreased to various degrees in the presence of above metal ions. This indicated that the presence of above ions reduced the binding constant of **3f**-HSA thereby causing **3f** to be rapidly cleared from the blood. This might lead to the need for more doses of **3f** to achieve the desired pharmacological effect.[41] Further, these results indicated that the quenching efficiency of **3f** was influenced by metal ions.

Conformational changes in secondary structure of the protein upon interaction

Absorption studies

The changes in the secondary structure of the protein and its complex formation with a small molecule can be investigated by absorption studies. Thus, to explore the changes in the environment around the protein structure, we have recorded absorption spectra of HSA in the presence of increasing amounts of **3f** (Fig. 7). It was evident from Fig. 7 that the absorbance of HSA increased upon the addition of increasing concentrations of **3f**. Thus, the change in polarity around the Trp residue and the change in peptide strand of HSA molecules was specified by the change in its λ_{max} and hence the change in hydrophobicity. This represents the binding between **3f** and protein that led to changes in the conformation of the protein.

3D fluorescence spectra

The maximum emission wavelength and fluorescence intensity of residues showed a close relation to the polarity of their microenvironment. In 3D-fluorescence spectroscopy, the excitation wavelength, emission wavelength and fluorescence intensity can be used as axes to investigate the integrated information of proteins. Thus, to attain more information on the binding of **3f** to HSA and to explore the conformational changes in the protein, 3D spectra of HSA were recorded in the presence and absence of **3f** and the corresponding spectra are shown in Fig. 8a and 8b.

Peaks 1 and 2 (Fig. 8) are the Rayleigh scattering peak ($\lambda_{ex} = \lambda_{em}$) and second-ordered scattering peaks ($\lambda_{ex} = 2\lambda_{em}$),[42] respectively. In addition, peak A ($\lambda_{ex}/\lambda_{em}$ = 230/316 nm) and peak B ($\lambda_{ex}/\lambda_{em}$ = 280/328 nm) were also observed in 3D fluorescence spectra. Peak A is due to $n \rightarrow \pi^*$ transition that is characteristic of the polypeptide backbone structure[43] of HSA while peak B represents the spectral characteristics of Trp and Tyrosine (Tyr) residues, since the protein predominantly displays the intrinsic fluorescence of Trp and Tyr residues upon excitation at 280 nm.[44] Analysis of Fig. 8 elucidated that the intensities of peaks A and B decreased to different degrees upon the addition of **3f**. The decrease in peak A demonstrated that the structure of the peptide strands has changed upon interaction with **3f** and that of peak B revealed that the interaction of **3f** with HSA induced some conformational changes in HSA, which were related to the hydrophobic microenvironment near Trp and Tyr residues. From these results, it could be inferred that HSA experienced a slight unfolding of the polypeptide chain of protein and conformational changes in the presence of **3f**.

Experimental Protocol

Synthesis of 1-[(2*E*)-3-phenylprop-2-enoyl]-1*H*-benzimidazole derivatives

Reported method[24] (Fig. 1) was followed to synthesize 1*H*-benzimidazole derivatives that involve drop wise addition of freshly prepared cinnamoyl chloride (1 eq.) to a solution containing substituted benzimidazoles (1 eq.) and sodium hydride (1.1 eq.) in THF at 0-5 °C. The reaction was carried out in an inert atmosphere. Then, the reaction mixture was allowed to attain ambient temperature and the stirring was continued. After the completion of the reaction, the volume of THF was reduced to half in *vacuo* and poured to crushed ice and the pH was adjusted to neutral. The separated solid was filtered, washed with water, dried and finally purification was achieved on a silica gel (60-120 mesh) column chromatography using ethyl acetate/hexane as the eluent. Characterization of synthesized molecules is given in supplementary information file.

Anticancer screening methodology

The evaluation of anticancer activity was carried out at National Cancer Institute (NCI) Bethesda, Maryland, USA, under the Developmental Therapeutic Program (DTP).[45] The human tumor cell lines of the cancer screening panel were grown in RPMI 1640 medium containing 5% fetal bovine serum and 2 mM L-glutamine. For a typical screening experiment, cells were inoculated into 96 well microtiter plates in 100 µL at plating densities ranging from 5,000 to 40,000 cells/wells depending on the doubling time of individual cell lines. After cell inoculation, the microtiter plates were incubated at 37 ºC, 5% CO_2, 95% air and 100% relative humidity for 24 h prior to addition of experimental drugs. After 24 h, two

plates of each cell line were fixed *in situ* with TCA, to represent a measurement of the cell population for each cell line at the time of drug addition (T_z). Experimental drugs were solubilized in dimethyl sulfoxide at 400-fold the desired final maximum test concentration and stored frozen prior to use. At the time of drug addition, an aliquot of frozen concentrate was thawed and diluted to twice the desired final maximum test concentration with complete medium containing 50 μg mL^{-1} gentamicin. Additional four, 10-fold or ½ log serial dilutions were made to provide a total of five drug concentrations plus control. Aliquots of 100 μL of these different drug dilutions were added to the appropriate microtiter wells containing 100 μL of medium, resulting in the required final drug concentrations. Following the drug addition, the plates were incubated for an additional 48 h at 37 °C, 5% CO_2, 95% air and 100% relative humidity. For adherent cells, the assay was terminated by the addition of cold TCA. Cells were fixed *in situ* by the gentle addition of 50 μL of cold 50% (w/v) TCA (final concentration, 10 % TCA) and incubated for 60 min at 4 ºC. The supernatant was discarded, and the plates were washed five times with tap water and air dried. Sulforhodamine B (SRB) solution (100 μL) at 0.4% (w/v) in 1% acetic acid was added to each well, and plates were incubated for 10 min at room temperature. After staining, the unbound dye was removed by washing five times with 1% acetic acid and the plates were air dried. Bound stain was subsequently solubilized with 10 mM trizma base, and the absorbance was read on an automated plate reader at a wavelength of 515 nm. For suspension cells, the methodology was the same except that the assay was terminated by fixing settled cells at the bottom of the wells by gently adding 50 μL of 80% TCA (final concentration, 16% TCA). Using the seven

absorbance measurements [time zero, (T_z), control growth, (C), and test growth in the presence of drug at five concentration levels (T_i)], the percentage growth was calculated at each of the drug concentration level. Percentage growth inhibition can be calculated using the following equation:

$[(T_i-T_z)/(C-T_z)] \times 100$ for concentrations for which $T_i \geq T_z$

$[(T_i-T_z)/T_z] \times 100$ for concentrations for which $T_i<T_z$.

Three dose response parameters were calculated for each experimental agent. Growth inhibition of 50% (GI_{50}) was calculated using the equation $[(T_i-T_z)/(C-T_z)] \times 100 = 50$, which is the drug concentration resulting in a 50% reduction in the net protein increase (as measured by SRB staining) in control cells during the drug incubation. The drug concentration resulting in a total growth inhibition (TGI) is calculated from $T_i = T_z$. The LC_{50} (concentration of drug resulting in a 50% reduction in the measured protein at the end of the drug treatment as compared to that at the beginning) indicating a net loss of cells following the treatment is calculated from $[(T_i-T_z)/T_z] \times 100 = -50$. Values were calculated for each of these three parameters if the level of activity was reached. However, if the effect was not reached or is exceeded, the value for that parameter was expressed as greater or lesser than the maximum or minimum concentration tested.

Materials and methods for the interaction and conformational studies of HSA in the presence of 3f

Steady state fluorescence spectra were performed on a Agilent technologies Cary Eclipse fluorescence spectrometer equipped with a Xenon flash lamp source and a Cary single cell peltier for temperature control. Absorbances were recorded on a Jasco

V-670 UV-vis spectrophotometer equipped with a 1.0 cm quartz cell. For emission spectra, excitation and emission slits with a band pass of 5.0 nm were used for all measurements. The excitation wavelength was set at 280 nm for HSA and emission spectra were recorded in the wavelength range of 285-500 nm.

HSA was purchased from Sigma-Aldrich, India and used without further purification. A stock solution of HSA was prepared by dissolving the appropriate amount of HSA (250 μM) in phosphate buffer of pH 7.4 in Millipore water, while those of synthesized compounds were prepared in 30% ethanol (25 μM). HSA solution was stored at 4 ºC. All measurements were carried out at the physiological pH of 7.4 using 0.1 M phosphate buffer. Fluorescence intensities were recorded by keeping the concentration of protein fixed at 2.5 μM and varying that of compound **3f** in the range of 0.25-2.00 μM at 288, 298 and 308 K. Absorption spectra were recorded in the range of 200-460 nm. The 3D fluorescence spectra were performed under the following conditions: the emission wavelength was recorded between 200 and 550 nm and the initial excitation wavelength was set at 200 nm with an increment of 10 nm up to 350 nm. Other scanning parameters were identical to those maintained for steady state fluorescence studies.

Displacement experiments were performed using different site probes *viz*., phenylbutazone, ibuprofen and digitoxin for site I, II and III, respectively. For this, the concentration of HSA and compound **3f** was maintained similarly as that maintained for steady state fluorescence measurements. The corresponding fluorescence intensities were recorded.

Fluorescence spectra of **3f**-HSA were recorded in the presence of some cations (at 0.25 μM) *viz*., K^+, Co^{2+}, Cu^{2+}, Ni^{2+}, Mn^{2+} and Zn^{2+} upon excitation at 280 nm.

Conclusions

The anticancer activity of synthesized molecules has been investigated against full NCI 60 cell panel at NCI, USA. Compound **3f** (NSC: 773404/1) was found to possess a considerable antiproliferative activity towards the majority of the human tumor cell lines and selected for five dose assays at 10-fold dilutions of five different concentrations. This compound was found to display a wide spectrum of antitumor activity against the nine tumor subpanels tested with selectivity ratios ranging from 0.79 to 1.53 and from 0.47 to 1.69 at GI_{50} and TGI levels, respectively. Single crystals of more potent anticancer active compound, **3f** were grown and their crystal parameters were studied. Further, *in vitro* studies on interactions of **3f** with HSA were carried out. Conformational changes in secondary structure of the protein upon interaction with **3f** have been studied by spectroscopic techniques. Static quenching mechanism was observed in the binding of **3f** to HSA. Based on site marker competitive experiments, the compound **3f** was proposed to bind to subdomain IIA in HSA. The thermodynamic parameters revealed that the hydrogen bond and van der Waals forces played a major role in the interaction between **3f** and HSA. Absorption and 3D-fluorescence studies confirmed the conformational changes in the secondary structure of protein upon interaction.

Acknowledgments

We are grateful to NCI, NIH, Bethesda, USA for selecting our samples for *in vitro* anticancer analysis under DTP. We wish to thank the University Grants

Commission (UGC), New Delhi [F. No. 14-3/2012 (NS/PE) dated 14-03-2012] for providing financial support under "*Antitumor activity: an integrated approach*" a focused area of UPE program. The authors also acknowledge the University Scientific Instrumentation Centre, Karnatak University, Dharwad for single crystal X-ray data.

References:

1 World Health Organization, World Cancer Report, 2008 http://apps.who.int/bookorders/anglais/detart1.jsp?codlan=1&codcol=76&codcch=26(accessed June 2015).

2 M.M. Gottesman, *Annu. Rev. Med.*,2002, **53**, 615-627.

3 Y.A. Luqmani, *Med. Princ. Pract.*,2005, **14**, 35-48.

4 H.M. Refaat, *Eur. J. Med. Chem.*,2010, **45**, 2949-2956.

5 A. M. Youssef, A.Malki, M.H. Badr, R.Y. Elbayaa and A.S. Sultan, *Med. Chem.*, 2012, **8**, 151-162.

6 Y. Bansal and O. Silakari, *Bioorg. Med. Chem.*,2012, **20**, 6208-6236.

7 H.S.A. Elzahabi, *Eur. J. Med. Chem.*,2011, **46**, 4025-4034.

8 V. Martinez, C. Burgos, J. Alvarez-Builla, G. Fernandez, A. Domingo, R. Garcia-Nieto, F. Gago, I. Manzanares, C. Cuevas and J.J. Vaquero, *J. Med. Chem.*,2004, **47**, 1136-1148.

9 A.R. Katritzky, D.O. Tymoshenko, D. Monteux, V. Vvedensky, G. Nikonov, C.B. Cooper and M. Deshpande, *J. Org. Chem.*,2000, **65**, 8059-8062.

10 R. Abonia, E. Cortes, B. Insuasty, J. Quiroga, M. Nogueras and J. Cobo, *Eur. J. Med. Chem.*,2011, **46**, 4062-4070.

11 D.G. O'Sullivan and A.K. Wallis, *J. Med. Chem.*, 1972, **15**, 103–104.

12 R. Zou, K.R. Ayres, J.C. Drach and L.B. Townsend, *J. Med. Chem.*,1996, **39**, 3477-3482.

13 S.L. Zhang, G.L.V. Damu, L. Zhang, R.X. Geng and C.H. Zhou, *Eur. J. Med. Chem.*,2012, **55**, 164-175.

14 J. Valdez, R. Cedillo, A.H. Campos, L. Yepez, F.H. Luis, G.N. Vazquez, A. Tapia, R. Cortes, M. Hernandez and R. Castillo, *Bioorg. Med. Chem. Lett.*,2002, **12**, 2221–2224.

15 M. Gaba, D. Singh, S. Singh, V. Sharma and P. Gaba, *Eur. J. Med. Chem.*,2010, **45**, 2245-2249.

16 S. Grabmann, B. Sadek, X. Ligneau, S. Elz, C.R. Ganellin, J.M. Arrang, J.C. Schwartz, H. Stark and W. Schunack, *Eur. J. Pharm. Sci.*,2002, **15**, 367–378.

17 K. V. Thimann, The auxins. In: M. B. Son, (ed.) Physiology of plant growth and development, McGrew-Hill, London, pp 2-45, 1969.

18 B. Z. Ahn and D. E. Sok, *Curr. Pharm. Design,* 1996, **2**, 247-262.

19 D. Raffa, B. Maggio, F. Plescia, S. Cascioferro, S. Plescia, M. V. Raimondi, G. Daidone, M. Tolomeo, S. Grimaudo, A. D. Cristina, R. M.Pipitone, R.Bai and E. Hamel, *Eur. J. Med. Chem.*, 2011, **46**, 2786-2796.

20 D.C. Carter and J.X. Ho, *Adv. Protein Chem.*,1994, **45**, 153-203.

21 H. N. Hou, Z. D.Qi, Y. W.OuYang, F. L. Liao, Y. Zhang and Y. Liu, *J. Pharm. Biomed. Anal.*,2008, **47**, 134–139.

22 T. Jr. Peters, *Adv. Protein Chem.*,1985, **37**, 161-245.

23 W.J. Jusko and M. Gretch, *Drug Metab. Rev.*,1976, **5**, 43–140.

24 V.K.A. Kalalbandi, J. Seetharamappa, U. Katrahalli and K.G. Bhat, *Eur. J. Med. Chem.*,2014, **79**, 194-202.

25 G.M. Sheldrick, ActaCrystallogr. A,2008, **64**, 112.

26 National Cancer Institute, Division of Cancer Treatment and Diagnosis,

http://dctd.cancer.gov/ProgramPages/dtp/tools_drug_discovery.htm (accessed June 2015).

27 A. R. Ali, E.R. El-Bendary, M.A. Ghaly and I.A. Shehata, *Eur. J. Med. Chem.*,2013, **69**, 908-919.

28 National Cancer Institute, DTP-COMPARE, http://dtp.nci.nih.gov/docs/compare/compare.html (accessed June 2015).

29 N. Kode, L. Chen, D. Murthy, D. Adewumi and S. Phadtare, *Eur. J. Med. Chem.*,2007, **42**, 327-333.

30 P. Corona, A. Carta, M. Loriga, G. Vitale and G. Paglietti, *Eur. J. Med. Chem.*,2009, **44**, 1579-1591.

31 S.A.F. Rostom, *Bioorg. Med. Chem.*,2006, **14**, 6475-6485.

32 E. Chew, A. A. Nagle, Y. Zhang, S. Scarmagnani, P. Palaniappan, T. D. Bradshaw, A. Holmgren and A. D. Westwell, *Free Radical Bio. Med.,* 2010, **48**, 98-111.

33 C.M. Cabello, W.B. Bair III, S.D. Lamore, S. Ley, A.S. Bause, S. Azimian and G.T. Wondrak, *Free Radical Bio. Med.*,2009, **46**, 220–231.

34 J. Lakowicz, in *Principles of Fluorescence Spectroscopy*, Plenum, New York, 2ndedn., 1999.

35 J.R. Brown, in *Albumin Structure, Function and Uses*, ed. V.M. Rosenoer, M. Oratz and M.A. Rothschild, Pergamon, Oxford, 1977, pp. 27-52b.

36 M.R. Eftink, in *Biophysical and Biochemical Aspects of Fluorescence Spectroscopy*, Plenum, New York, 1991.

37 X.Z. Feng, Z. Lin, L.J. Yang, C. Wang and C. L. Bai, *Talanta*, 1998, **47**, 1223-1229.

38 J.Tang, F. Luan and X.Chen, *Bioorg. Med. Chem.*,2006, **14**, 3210-3217.

39 P.D. Ross and S. Subramanian, *Biochemistry*,1981, **20**,3096-3102.

40 G. Sudlow, D.J. Birkett and D.N. Wade, *Mol. Pharmacol.*,1975, **11**, 824-832.

41 F.L. Cui, J. Fan, J.P. Li and Z. Hu, *Bioorg. Med. Chem.*,2004, **12**, 151-157.

42 Y. Yue, J. Liu, J. Fan and X. Yao, *J. Pharm. Biomed. Anal.*,2011, **56**, 336-342.

43 A. N. Glazer and E.L. Smith, *J. Biol. Chem.*,1961, **236**, 2942-2947.

44 G. W. Zhang, Q. M. Que, J. H. Pan and J. B.Guo, *J. Mol. Struct.*,2008, **881**, 132-138.

45 Developmental Therapeutics Program NCI/NIH, Screening services, http://dtp.nci.nih.gov/branches/btb/ivclsp.html (accessed June 2015).

Glossary

3D – Three dimensional

CCDC - Cambridge Crystallographic Data Centre

COMPARE - A computerized, pattern recognition algorithm which has considerable utility in the evaluation and exploitation of data generated by the NCI screen.

GI_{50} - The concentration for 50% of maximal growth inhibition of cell proliferation.

HPLC – High Performance Liquid Chromatography

HSA – Human Serum Albumin

LC_{50} - The concentration for killing 50% of disease cell (Lethal Concentration)

MID – Mid point

NCI – National Cancer Institute

NSC – National Service Centre

ORTEP - Oak Ridge Thermal Ellipsoid Plot

SAR – Structure Activity Relationship

SRB - Sulforhodamine B

TGI - The concentration for total growth inhibition of cell proliferation.

THF – Tetrahydrofuran

Trp – Tryptophan

Tyr – Tyrosine

Table Captions

Table 1 Crystal and structure refinement data of **3f**

Table 2 One dose mean graph of nine different cancer cell types of compound **3f (NSC: 773404/1)**.

Table 3 NCI *in vitro* testing results of compound **3f (NSC: 773404/1)** at five dose level in μM.

Table 4 Binding and thermodynamic parameters of **3f**-HSA system.

Table 5 Effect of common ions on the binding of **3f** to HSA at 303 K.

Table 1 Crystal and structure refinement data of **3f**

Parameter	
Empirical formula	$C_{22}H_{15}ClN_2O$
Formula weight	358.82
Temperature	296 K
Crystal size	0.30x0.20x0.20 mm
Crystal color	Colorless
Crystal system	Monoclinc
Space group	$P2_1/c$
Unit cell dimensions	a = 13.5275(10) Å, α = 90° b = 7.5746(5) Å, β = 111.098(2)° c = 18.3908(11) Å, γ = 90°
Limiting indices	-15<=h<=14, -8<=k<=8, -20<=l<=20
Volume	1758.1 (2) $Å^3$
Z, Calculated density	4, 1.359 mg/m^3
Reflections collected	10366
No. of independent reflections	2764 [R(int) = 0.0330]
Data/Restraints/Paramaeters	2764 / 0 / 236
Final R indices [I> 2σ(I)]	R1 = 0.0395, wR2 = 0.1016
R indices (all data)	R1 = 0.0591, wR2 = 0.1159
Measurements	Bruker SMART APEX2 CCD Diffractometer
Refinement program	SHELXL-97 (Sheldrick, 2008)
Refinement method	Full-matrix least squares on F^2
Goodness of fit	1.008
CCDC deposit number	CCDC 1018656

Table 2 One dose mean graph of nine different cancer cell types of compound **3f (NSC: 773404/1)**.

Panel	Cell lines	Growth percent	Growth inhibition
Leukemia	CCRF-CEM	-23.88	Cytotoxic
	HL-60 (TB)	-3.97	Cytotoxic
	K-562	39.78	60.22
	MOLT-4	21.93	78.07
	RPMI-8226	-31.13	Cytotoxic
Non-Small Cell Lung Cancer	A549/ATCC	-4.99	Cytotoxic
	HOP-62	-48.81	Cytotoxic
	HOP-92	-39.42	Cytotoxic
	NCI-H226	-55.28	Cytotoxic
	NCI-H23	-24.46	Cytotoxic
	NCI-H322M	45.05	54.95
	NCI-H460	0.54	99.46
	NCI-H522	-72.37	Cytotoxic
Colon Cancer	COLO 205	-60.78	Cytotoxic
	HCC-2998	5.08	94.92
	HCT-116	-71.46	Cytotoxic
	HCT-15	-24.78	Cytotoxic
	HT29	-40.61	Cytotoxic
	KM12	-62.91	Cytotoxic
	SW-620	-55.08	Cytotoxic
CNS Cancer	SF-268	-11.85	Cytotoxic
	SF-295	-51.99	Cytotoxic
	SF-539	-48.44	Cytotoxic
	SNB-19	41.12	58.88
	SNB-75	18.07	81.93
	U251	-0.39	Cytotoxic
Melanoma	LOX IMVI	-82.92	Cytotoxic
	MALME-3M	15.88	84.12
	M14	-37.34	Cytotoxic
	MDA-MB-435	-44.30	Cytotoxic
	SK-MEL-2	-36.05	Cytotoxic
	SK-MEL-28	-65.41	Cytotoxic
	SK-MEL-5	-70.59	Cytotoxic
	UACC-257	-64.42	Cytotoxic
	UACC-62	-84.68	Cytotoxic
Ovarian Cancer	IGROV-1	10.38	89.62
	OVCAR-3	-57.18	Cytotoxic
	OVCAR-4	30.04	69.96
	OVCAR-5	-48.09	Cytotoxic
	OVCAR-8	-31.30	Cytotoxic
	NCI/ADR-RES	10.78	89.22
	SK-OV-3	23.95	76.05
Renal Cancer	786-0	-17.65	Cytotoxic
	A498	-14.61	Cytotoxic
	ACHN	-49.87	Cytotoxic
	CAKI-1	-39.45	Cytotoxic
	RXF-393	-65.21	Cytotoxic
	SN12C	-48.49	Cytotoxic
	TK-10	18.58	81.42
	UO-31	-38.98	Cytotoxic
Prostate Cancer	PC-3	6.09	93.91
	DU-145	11.13	88.87
Breast Cancer	MCF-7	10.29	89.71
	MDA-MB-231/ATCC	-26.52	Cytotoxic
	HS 578T	19.97	80.03
	BT-549	-50.47	Cytotoxic
	T-47D	-4.25	Cytotoxic
	MDA-MB-468	-6.61	Cytotoxic

Table 3 NCI in vitro testing results of compound **3f (NSC: 773404/1)** at five dose level in μM.

Panel	Cell lines	GI_{50}			TGI			LC_{50}
		Conc. Per Cell line	Sub Panel MID[b]	Selectivity ratio (MID[a] : MID[b])	Conc. Per Cell line	Sub Panel MID[d]	Selectivity ratio (MID[c] : MID[d])	
Leukemia	CCRF-CEM	0.73	1.06	1.53	3.45	5.43	1.13	>100
	HL-60 (TB)	1.40			4.88			>100
	K-562	2.09			11.8			>100
	MOLT-4	1.13			6.73			>100
	RPMI-8226	0.61			3.82			>100
	SR	0.38			1.88			>100
Non-Small Cell Lung Cancer	A549/ATCC	1.89	1.86	0.87	7.30	4.98	1.23	35.1
	HOP-62	2.72			5.17			9.81
	HOP-92	1.46			3.82			10.0
	NCI-H226	2.17			6.00			>100
	NCI-H23	1.91			4.89			20.0
	NCI-H322M	1.96			6.52			25.5
	NCI-H460	1.53			3.50			8.04
	NCI-H522	1.23			2.64			5.65
Colon Cancer	COLO 205	1.41	1.45	1.12	2.78	3.98	1.54	5.49
	HCC-2998	1.80			3.45			6.61
	HCT-116	1.21			2.88			6.90
	HCT-15	1.34			7.05			29.8
	HT29	1.51			3.71			9.16
	KM12	1.44			2.93			5.97
	SW-620	1.45			5.03			27.9
CNS Cancer	SF-268	2.10	2.04	0.79	6.14	5.89	1.04	42.5
	SF-295	2.50			6.46			26.1
	SF-539	1.47			2.92			5.79
	SNB-19	3.13			12.8			40.5
	SNB-75	1.44			3.77			9.91
	U251	1.60			3.22			6.50
Melanoma	LOX IMVI	0.59	1.47	1.10	1.91	3.63	1.69	4.77
	MALME-3M	1.63			5.74			26.0
	M14	1.90			5.05			19.6
	MDA-MB-435	1.11			3.04			8.32
	SK-MEL-2	2.10			4.35			9.02
	SK-MEL-28	1.49			3.22			6.92
	SK-MEL-5	1.64			3.12			5.93
	UACC-257	1.47			3.42			7.93
	UACC-62	1.27			2.88			6.53
Ovarian Cancer	IGROV-1	1.95	1.78	0.91	4.63	12.92	0.47	13.4
	OVCAR-3	1.11			2.64			6.29
	OVCAR-4	3.01			1.67			49.7
	OVCAR-5	1.74			4.21			10.5
	OVCAR-8	0.75			10.3			62.1
	NCI/ADR-RES	1.49			61.3			>100
	SK-OV-3	2.43			5.71			18.0
Renal Cancer	786-0	2.05	1.51	1.07	7.63	5.36	1.14	28.4

	A498	1.17			2.56			5.62
	ACHN	1.18			10.0			31.7
	RXF-393	1.32			3.12			7.37
	SN12C	1.39			2.76			5.46
	TK-10	2.35			7.93			28.0
	UO-31	1.10			3.55			12.9
Prostate Cancer	PC-3	1.91	1.86	0.87	6.73	5.83	1.05	36.3
	DU-145	1.80			4.93			17.0
Breast Cancer	MCF-7	1.01	1.73	0.93	9.92	8.03	0.76	55.5
	MDA-MB-231/ATCC	1.88			5.18			25.4
	HS 578T	2.57			17.9			>100
	BT-549	1.67			3.22			6.18
	T-47D	1.73			7.68			57.5
	MDA-MB-468	1.52			4.32			23.7
MID[a]		1.62		MID[c]	6.14			

Table 4 Binding and thermodynamic parameters of **3f**-HSA system.

System	T (K)	K_{SV} ($L\ mol^{-1}$)	R^2	K (mol^{-1})	n	ΔHº ($kJ\ mol^{-1}$)	ΔSº ($J\ mol^{-1}\ K^{-1}$)	ΔGº ($kJ\ mol^{-1}$)
3f-HSA	288	$2.03x10^5$	0.9908	$2.24x10^5$	1.00	-132.0	-356.1	-29.5
	298	$1.37x10^5$	0.9899	$3.20x10^4$	0.88			-25.7
	308	$1.14x10^5$	0.9976	$6.27x10^3$	0.77			-22.4

Table 5 Effect of common ions on the binding of **3f** to HSA at 303 K.

System	K (10^3, mol^{-1})
3f -HSA	5.68
3f-HSA-Co^{2+}	4.09
3f-HSA-Cu^{2+}	2.44
3f-HSA-K^{+}	4.21
3f-HSA-Mn^{2+}	3.85
3f-HSA-Ni^{2+}	5.35
3f-HSA-Zn^{2+}	2.26

Figure captions

Fig. 1 Synthetic route for the synthesis of 1*H*-benzimidazole

Fig. 2 (**a**) ORTEP diagram of compound **3f ;** (**b**) Diagram showing intermolecular interactions.

Fig. 3 Dose response curves (% growth verses sample concentration at NCI fixed protocol, μM) obtained from the NCI's *in vitro* disease-oriented human tumor cells line of compound (**3f**) on nine cancer disease.

Fig. 4 Fluorescence quenching spectra of HSA (2.5 μM) in the presence of increasing amounts of compound **3f** (a-i: 0, 0.25, 0.50, 0.75, 1.00, 1.25, 1.50, 1.75 and 2.00 μM) upon excitation at 280 nm.

Fig. 5 The Stern-Volmer curves for quenching of **3f** with HSA at different temperatures.

Fig. 6 The van't Hoff plot for the binding of **3f** with HSA.

Fig. 7 Absorption spectra of 5 μM HSA (a) in the presence of increasing concentrations of **3f** (b-i: 0.25, 0.50, 0.75, 1.00, 1.25, 1.50, 1.75 and 2.00 μM). (x) Indicates 0.25 μM of **3f** only.

Fig. 8 3D fluorescence spectra of (a) HSA (2.5 μM) and (b) HSA + **3f** (2.5 μM).

Fig. 1 Synthetic route for the synthesis of 1*H*-benzimidazole

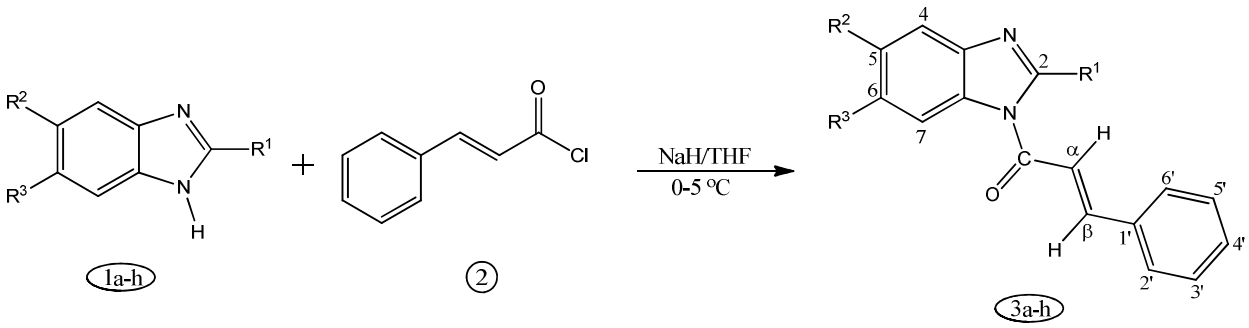

	R^1	R^2	R^3
a	CH_3	H	H
b	H	CH_3	CH_3
c	H	H	CH_3
d	C_6H_5	H	H

	R^1	R^2	R^3
e	4-OCH_3-C_6H_4	H	H
f	4-Cl-C_6H_4	H	H
g	2-OH-C_6H_4	H	H
h	4-OH-C_6H_4	H	H

Fig. 2 (**a**) ORTEP diagram of compound **3f;** (**b**) Diagram showing intermolecular interactions.

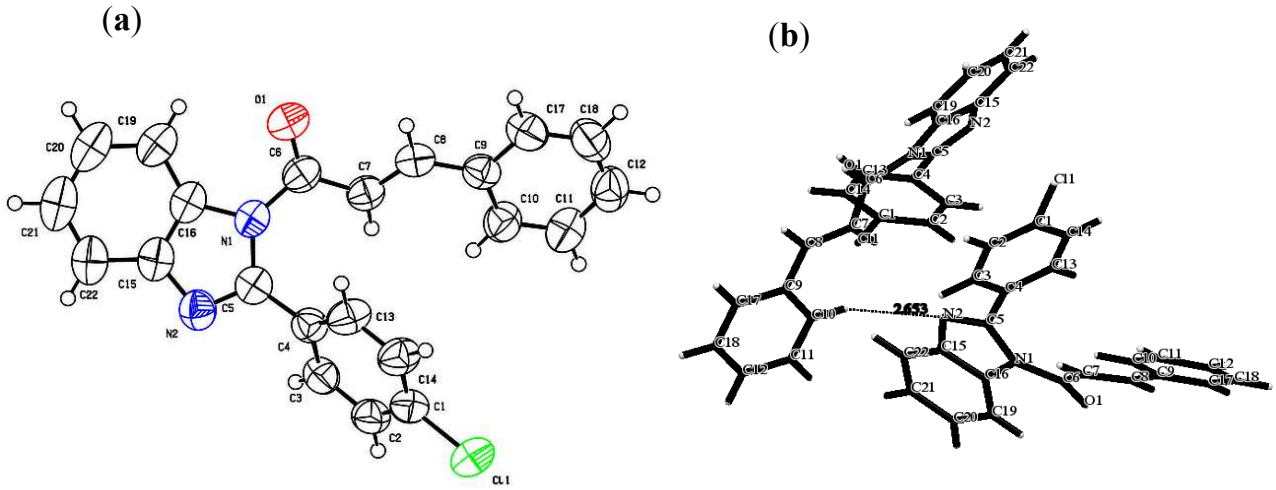

Fig. 3 Dose response curves (% growth verses sample concentration at NCI fixed protocol, μM) obtained from the NCI's *in vitro* disease-oriented human tumor cells line of compound (**3f**) on nine cancer disease.

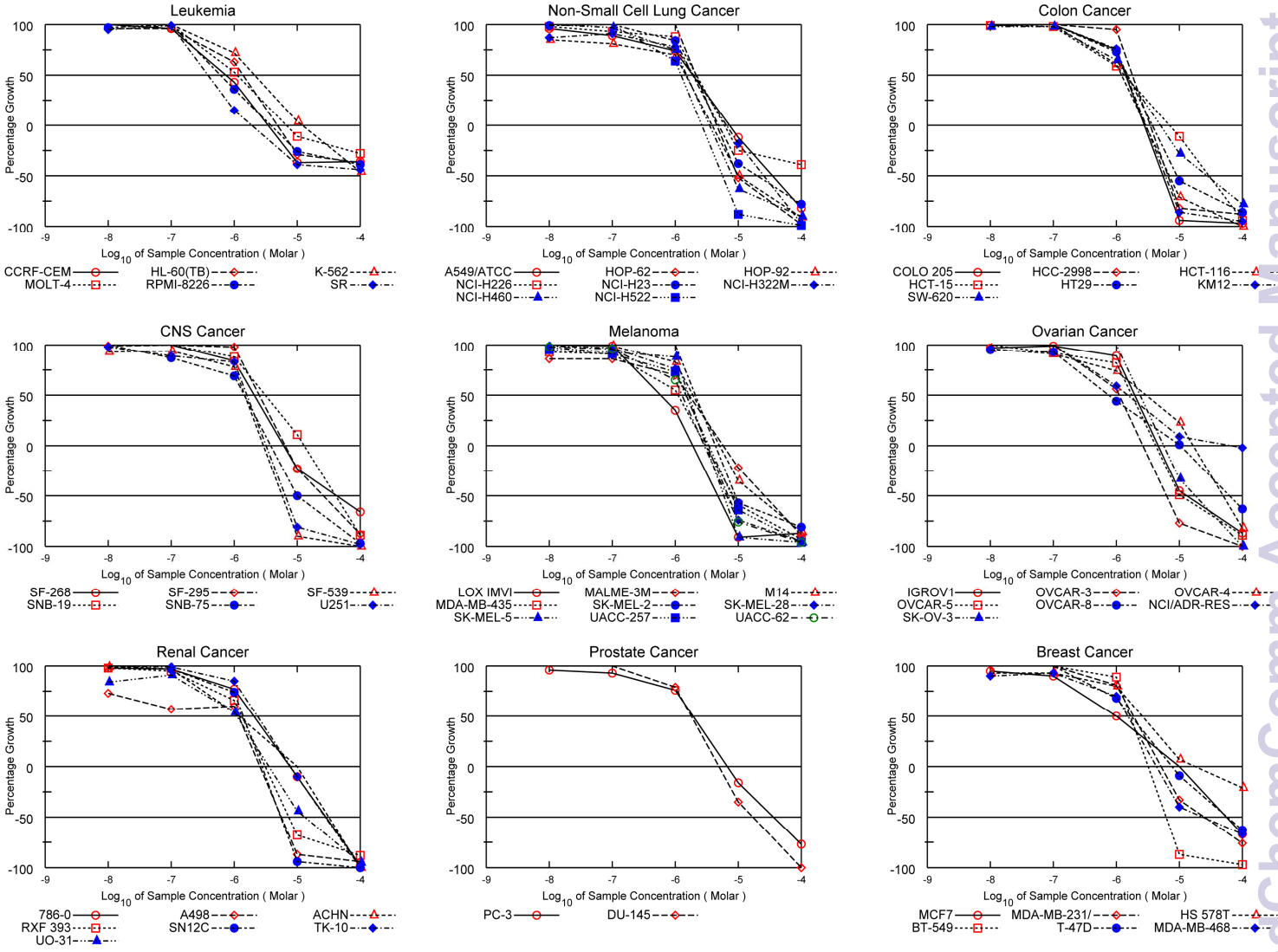

Fig. 4 Fluorescence quenching spectra of HSA (2.5 μM) in the presence of increasing amounts of compound **3f** (a-i: 0, 0.25, 0.50, 0.75, 1.00, 1.25, 1.50, 1.75 and 2.00 μM) upon excitation at 280 nm.

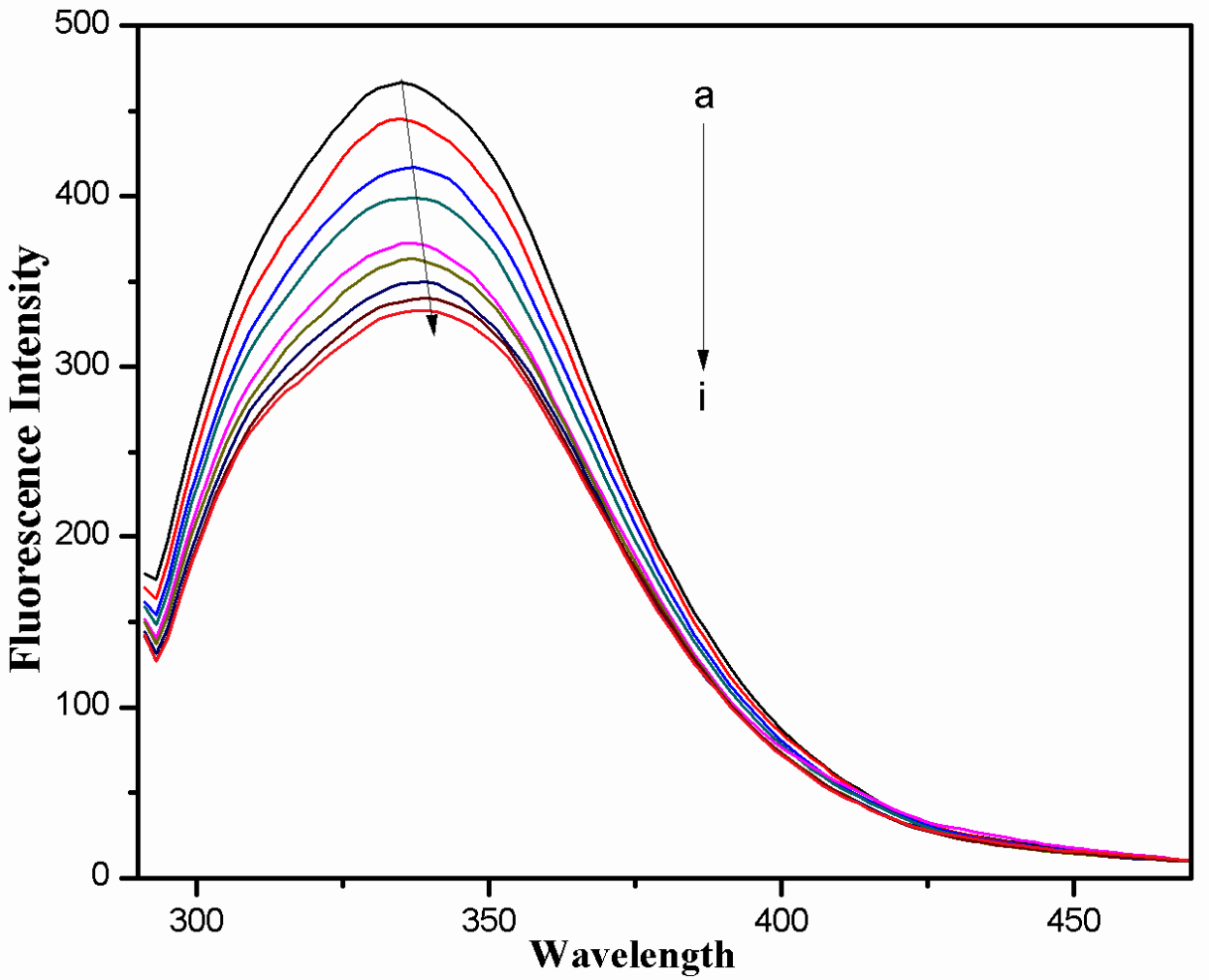

Fig. 5 The Stern-Volmer curves for quenching of **3f** with HSA at different temperatures.

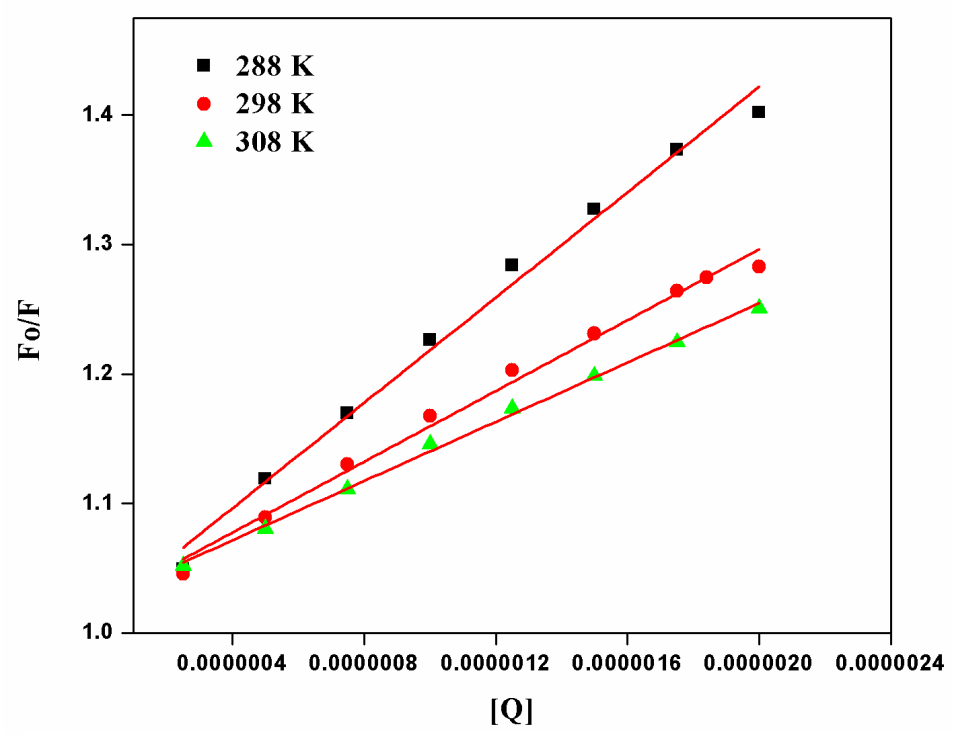

Fig. 6 The van't Hoff plot for the binding of **3f** with HSA.

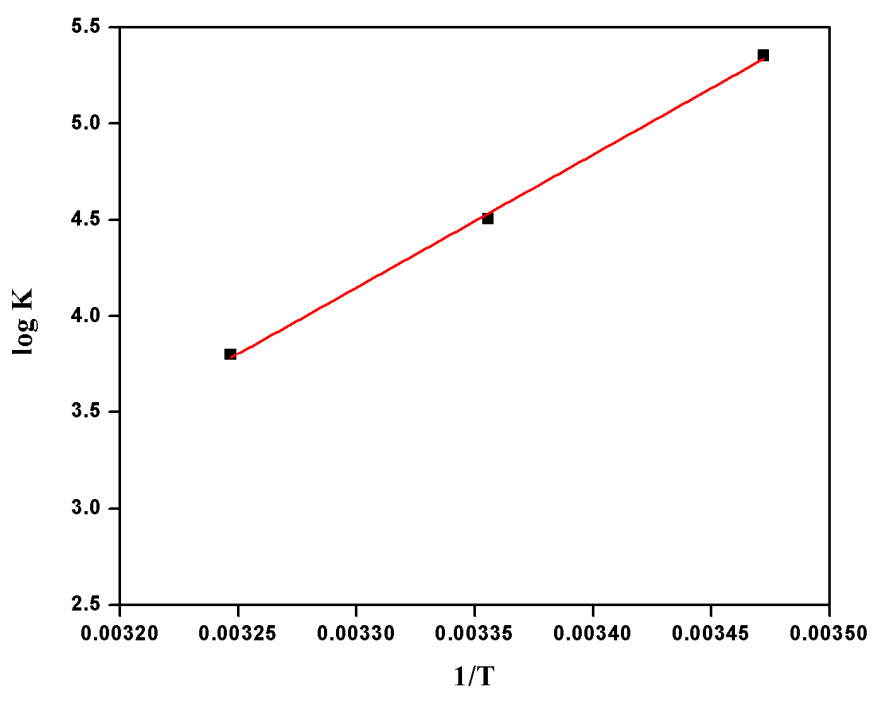

Fig. 7 Absorption spectra of 5 μM HSA (a) in the presence of increasing concentrations of **3f** (b-i: 0.25, 0.50, 0.75, 1.00, 1.25, 1.50, 1.75 and 2.00 μM). (x) Indicates 0.25 μM of **3f** only.

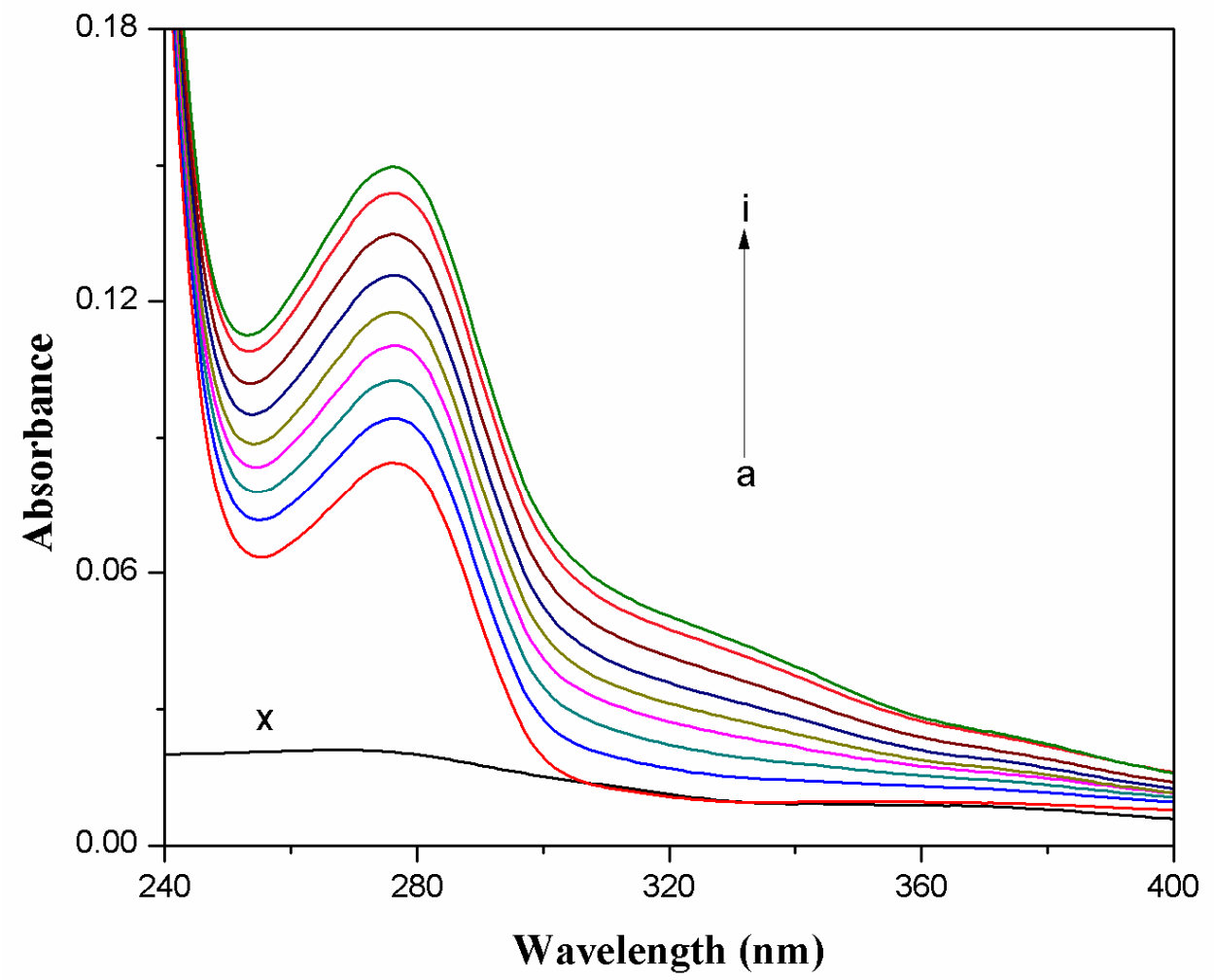

Fig. 8 3D fluorescence spectra of (a) HSA (2.5 μM) and (b) HSA + **3f** (2.5 μM).

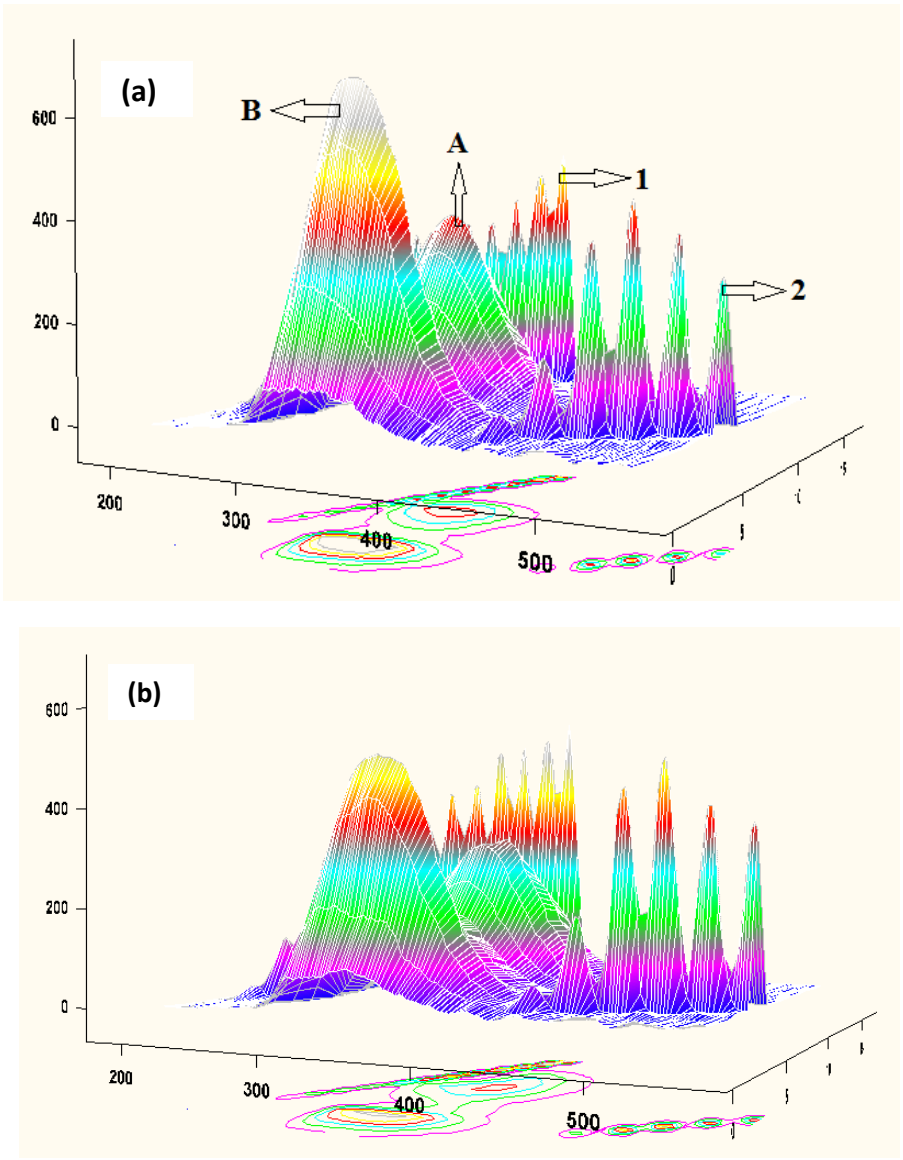

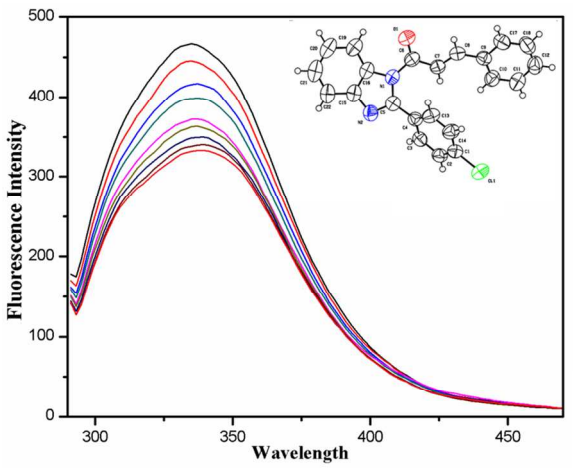

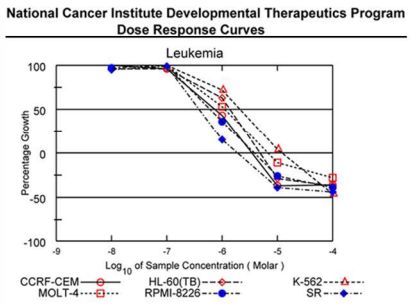

¬ Anticancer activity of 1H-benzimidazoles was studied against NCI60 cell panel
¬ Compound 3f showed antitumor activity with good to moderate selectivity ratio
¬ Mechanism of interaction of 3f with protein was studied by spectral methods
¬ Compound 3f was proposed to bind to site I of subdomain IIA in the protein

351x169mm (96 x 96 DPI)